Metrology State-of-the-art and Challenges in Broadband Phase-sensitive Terahertz Measurements

Mira Naftaly[1], Roland G. Clarke[2] *Member, IEEE*, David A. Humphreys[1] *Senior Member, IEEE*, and Nick M. Ridler[1] *Fellow, IEEE*

[1]National Physical Laboratory, Teddington, UK; [2]University of Leeds, Leeds, UK

Abstract

The two main modalities for making broadband phase-sensitive measurements at terahertz frequencies are Vector Network Analyzers (VNA) and Time Domain Spectrometers (TDS). These measuring instruments have separate and fundamentally different operating principles and methodologies, and they serve very different application spaces. The different architectures give rise to different measurement challenges and metrological solutions. This article reviews these two measurement techniques and discusses the different issues involved in making measurements using these systems. Calibration, verification and measurement traceability issues are reviewed, along with other major challenges facing these instrument architectures in the years to come. The differences in, and similarities between, the two measurement methods are discussed and analysed. Finally, the operating principles of Electro-Optic Sampling (EOS) are briefly discussed. This technique has some similarities to TDS and shares application space with the VNA.

1. Introduction

In recent times, the so-called "terahertz gap" in the electromagnetic spectrum between electronics and photonics measurements has been bridged from both directions, with an ever-extending frequency overlap region being made accessible by frequency extensions in both the electronics and photonics measurement techniques. Despite this, however, the two technologies co-exist in mutual isolation, with little communication, let alone cross-fertilization, kept apart by both instrumental incompatibilities and differing areas of application. Establishing co-operation and inter-comparability between the electronics and photonics measurement techniques is therefore one of the challenges of terahertz metrology.

The main platform for electronics THz measurements is the Vector Network Analyzer (VNA), which is an extension to higher frequencies of instrumentation first developed for testing lower-frequency (i.e. at MHz and GHz frequencies) devices and circuits. A VNA operates in the frequency domain, measuring the amplitude and phase of a signal interacting with a device-under-test (DUT); both transmitted and reflected signals are measured simultaneously, with the frequency being swept through the measurement band, providing frequency-dependent data. Historically, for these lower-frequency measurements, DUTs were connected to the VNA via coaxial cables fitted with standardized coaxial connectors. More recently, with the extension of VNAs to higher frequencies (millimeter-wave and THz frequencies), frequency extender heads fitted with standardized rectangular metal waveguides have been developed for these measurements. The frequency extender heads generate harmonics of the source fundamental frequency. A harmonic at the appropriate frequency is then used as the test signal, followed by harmonic mixing to enable the VNA's receiver circuitry to be employed in the usual way. True to their origins, in the THz region, VNAs are still mostly employed to study the performance of devices and components, which are coupled to the instrument via the waveguide test ports. As a long-established instrumentation platform, the VNA has well-developed calibration procedures and

calibration standards. Metrological challenges arise from the small dimensions of THz components and the engineering difficulties of manufacturing and assembling these components (including the VNA waveguide test ports) with the required precision.

The predominant technique in optical THz measurements is Time-Domain Spectroscopy (TDS). Invented in the early 1990s and having gained wide acceptance in the last decade, it is yet another technique in the long and illustrious tradition of optical spectroscopy, and is a laser-based approach, using "ultra-fast" pulsed lasers with pulse lengths of 100 fs or less. TDS operates in the time-domain, generating and detecting broadband pulses of THz radiation, each containing frequencies from < 0.1 THz up to 20 THz, whose amplitude and phase are recorded in the time-domain and whose spectral information is obtained by applying Fourier Transform. The sample is placed in the THz beam, and its optical properties are measured in transmission or reflection, using procedures similar to other spectroscopic methods. Note the names: TDS is used to study material "samples"; whereas the VNA primarily tests DUTs. In TDS, as in other spectrometers, the radiation propagates and interacts with the sample in free space; and the technique is used to study materials or substances (rather than devices). TDS is not only a relatively recent and novel technique, but it also possesses several unique features not encountered in other types of spectroscopy. For these reasons it currently lacks a commonly accepted standard measurement methodology and calibration is rarely considered or performed. The main metrological challenge for TDS is therefore to establish standardized procedures. Electro-Optic Sampling (EOS) is closely related to TDS, as regards measurement techniques, but is also akin to VNA in that it tests devices and circuits. Its metrological issues, however, are similar to those of TDS, with some added aspects of signal coupling to circuits.

In this paper we review the measurement techniques of VNA, TDS and EOS, and discuss issues of system performance, calibration, and their similarities and differences.

2. Terahertz Vector Network Analyzers

The VNA has traditionally been understood as an instrument designed to measure the complex (vector) scattering of electromagnetic signals incident on a test device (the 'network'). This concept utilizes the notion of 'ports' which define the interfaces through which signals flow into, and out from, the DUT. The measurement quantities are therefore the magnitude and phase of the propagating signals incident on, and scattered from, each port. The VNA forms ratios of these quantities in order to present scattering coefficients for the DUT. These are more often referred to as the scattering parameters (or 'S-parameters') familiar to the radio-frequency (RF) and microwave industry.

The scattering parameter approach requires that the incident and emergent signal amplitudes are normalized to the travelling-wave impedance for each port [1]. This means that the scattered signals between the ports are directly related to intuitive concepts such as the reflection and transmission properties of the DUT. The resulting scattering parameters may also be represented as a matrix of scattering coefficients. Providing the DUT is an electrically linear network, this will produce the satisfying result of a symmetrical scattering matrix for reciprocal networks, and it will also have a meaningful relationship to the flow of power into, and out from, the DUT [1]. More precise definitions of these terms can be found in [2].

Determining the DUT's scattering parameters allows a range of other parameters to be computed directly (for example, the propagation delay through the DUT, which is obtained by differentiating the transmission phase with respect to frequency). Time-domain measurements are also possible by applying the appropriate transforms to the measured frequency-domain scattering parameter data.

2.1 VNA measurement ports

Multiport VNAs are becoming commonplace for RF and microwave frequencies, but millimeter-wave and THz VNAs are usually two-port instruments. This means that they are useful for measuring the reflection and transmission behavior of one-port and two-port DUTs, for example: antennas, filters, amplifiers and signal-transmission structures. The ports may take several physical forms, but ordinarily some form of guided wave medium is implied. Whilst co-axial connectors and cables are employed at low frequencies (typically, below 100 GHz) it is common practice to use rectangular metallic waveguides at higher frequencies. Certainly, this is the case above 100 GHz, where there are well-established standards for the waveguide sizes and interconnecting flange details [3]. The choice of standardized rectangular waveguide sizes for millimeter-wave and THz frequencies, along with the associated frequency bands and interconnecting flange designs, has been reviewed during the past decade [4, 5]. A new IEEE standard has recently been introduced [6, 7] which defines a scalable approach suited to frequencies well into the THz regime.

The DUT may be any passive or active electronic circuit with appropriately specified measurement ports, which are not necessarily limited to metallic waveguides. This means that VNAs may also be employed for free-space measurement techniques using quasi-optical arrangements. With suitable analysis of the measurement data, applications can be extended to include materials characterization [8]. A further application for VNAs, which is convenient for characterizing the electrical behavior of semiconductor devices, is to make direct 'on-wafer' measurements. At millimeter-wave and THz frequencies, this has been accomplished using micro-machined contact probes [9] or via free-space focused beams [10]. This has led to the development of methods for characterizing transistors at millimeter-wave and terahertz frequencies [11]. In all of these VNA application environments, the ports are defined spatially and electrically to constitute the measurement reference planes.

2.2 VNA architecture

A VNA will normally use a continuous-wave (CW) signal source to provide the test stimulus. The stability, frequency-accuracy and power level of the source all contribute to the measurement quality. Early VNAs used backward-wave oscillators or Yttrium-Iron-Garnet 'YIG-tuned' oscillators to form a swept-frequency source. Modern VNAs use synthesized sources based on various frequency multiplication techniques. For millimeter-wave and THz systems, these sources usually take the form of harmonic multipliers, mostly based on Schottky diodes, such as those described in [12]. The harmonic mixer is then driven by the much lower-frequency, synthesized source.

Fundamental to the VNA instrument is the need to (a) distinguish between, and (b) measure, the incident (reference) and emerging reflected/transmitted (test) signals. To achieve the first of these goals, various 'directional' devices (e.g. directional couplers) have been employed. These are usually based on four-port waveguide junctions (for example, multi-hole waveguide couplers [13]). The directional couplers are used to extract a sample of the incident and emerging signals which form the basis of the scattering parameter measurements. Acquiring the magnitude and phase of these reference and test signals requires down-conversion (heterodyning) to intermediate frequencies (IF) where the magnitude and phase of the signals can be directly sampled (digitized). This approach succeeds because the frequency translation of both the reference and test signals preserves the phase relationships among the signals. THz VNAs typically use sub-harmonic mixers for this purpose, which permit a lower local oscillator (LO) frequency [14] – see Fig. 1. A more detailed discussion concerning the advantages of heterodyne detection, including the high dynamic range that can be achieved using narrowband filtering, can be

found in [15]. More detail relating to the application of heterodyne detection to terahertz VNA architectures, and the typically achievable dynamic range, has been given in [16, 17]. Fig. 2 shows the typical dynamic range, for a VNA operating from 750 GHz to 1.1 THz, in terms of the measured magnitudes of the transmission coefficients, S_{21} and S_{12}, when no device is connected between the two VNA test ports.
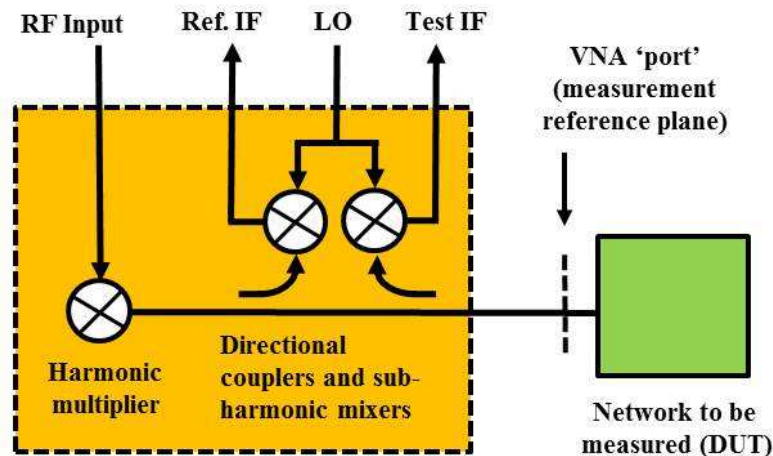
Fig. 1: THz VNA architecture. Shown here is a single measurement 'port' with the THz stimulus signal produced by a harmonic multiplier and directionally-coupled 'test' (reflected) and reference (incident) signals down-converted to IF signals via sub-harmonic mixers.
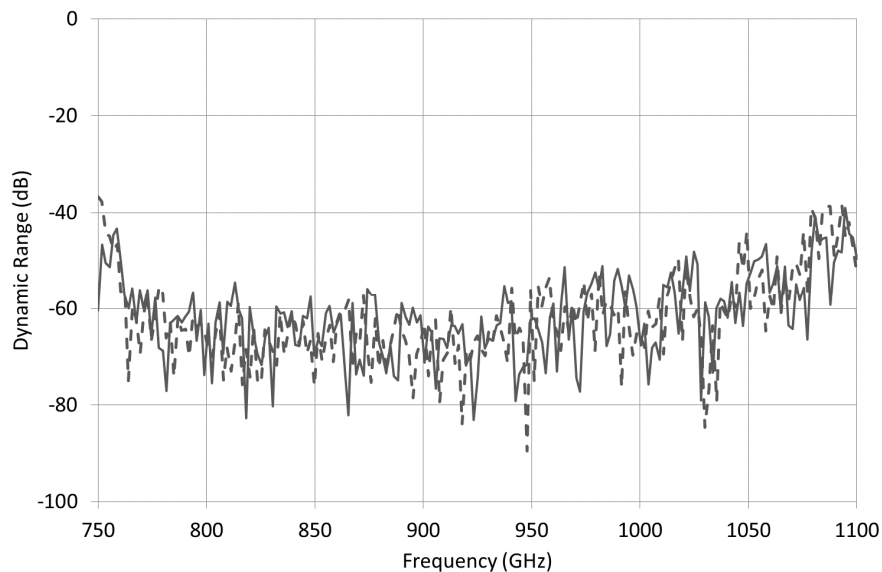
Fig. 2: Typical measured dynamic range for a VNA operating from 750 GHz to 1.1 THz, in the WM-250 waveguide size [6], with the VNA IF bandwidth was set to 30 Hz. The solid line shows the magnitude of the S_{21} response; the dashed line shows the magnitude of the S_{12} response

Millimeter-wave VNA systems have been in use for more than two decades, with systems operating at frequencies up to 325 GHz [18]. They are usually marketed as 'millimeter-wave extender heads' which are intended to be used in conjunction with a standard (RF/microwave) VNA. The extender heads

4

contain the harmonic multipliers for generating the stimulus signals, the sub-harmonic mixers used for the down-conversion of measurement signals and the signal separation devices (directional couplers). The VNA instrument continues to operate with signals in the 10 GHz to 20 GHz range and provides further stages of frequency down-conversion as required. This same operating principle has been applied in recent years to enable VNA systems to operate at submillimeter-wave (i.e. THz) frequencies – see, for example, Fig. 3.

Fig. 3: Typical VNA system for THz metrology. This instrument operates in the 0.75 THz to 1.1 THz waveguide band and is located at the University of Leeds, UK. The two 'black boxes' in the foreground are t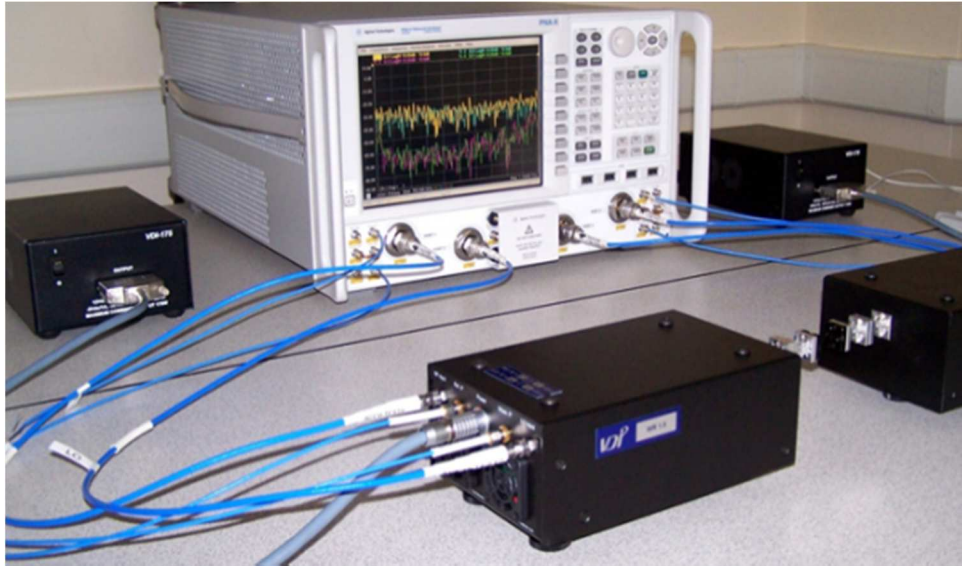he extender heads, shown inter-connected with sections of rectangular waveguide. The co-axial cables carry lower frequency signals to and from the VNA in the background.

Alternative VNA system architectures have also been proposed. The so-called six-port VNA [19, 20] utilizes a technique which allows the mapping of scalar power measurements to the complex scattering parameter quantities. This avoids the need for heterodyning the measurement signals, although it does not avoid the need for a stable CW stimulus signal at the desired measurement frequency. Also, the lack of coherent detection can lead to erroneous measurements if multiple frequency components are present in the test signal. Some specialized system architectures have also been described which are dedicated to millimeter-wave or THz VNA measurements, for example, those described in [21].

2.3 Calibration

The typical VNA architecture discussed above necessarily introduces a number of systematic errors. These are inevitable due to the possibility of different port impedances, measurement signal path losses, phase shifts, internal reflections, and factors such as imbalance in the directional couplers that form the test/stimulus ratios. However, providing all of these sources of error remain linear, it is possible to combine them into a reduced set of systematic errors which are relatively straightforward to correct through a calibration procedure.

Early techniques for performing such a VNA calibration relied on measuring a set of 'standards' with well-known scattering parameters. This technique is sometimes referred to as the 'short-open-load-

through' (SOLT) method [22]. A substantial improvement in calibration accuracy, and one which is particularly convenient for waveguide metrology, came in the form of the 'through-reflect-line (TRL) technique introduced in the 1970s [23]. The elegance of this technique derives from the fact that the only calibration standard that must have well-known properties is the 'through', which is simply a zero-length transmission path. This is easily satisfied in a genderless inter-connection environment such as rectangular waveguide, where the measurement reference planes are directly mated. This forms a path where the transmission loss and delay are both assumed to be zero. The TRL calibration algorithm does suffer from one limitation, namely that the 'line' standard (a non-zero-length transmission path) must not exhibit a signal phase-shift which differs from the 'through' standard by exactly $m \times \pi$ radians (where m is any integer). This imposes restrictions on the useful bandwidth of the line standard which is ordinarily realized by a short section of waveguide. For millimeter-wave and THz systems, this limitation also presents a practical difficulty, since the physical length of the waveguide 'line' required at 1 THz is typically in the region of 100 μm.

One proposed solution is a variant of TRL known as the 'line-reflect-line' (LRL) technique where the through standard is replaced by another non-zero-length 'line' [24]. The only requirement now is that the phase-shift between the two line lengths must not differ by $m \times \pi$ radians, which allows the use of longer lines. However, consistent with the TRL calibration technique from which it is derived, the first line standard in LRL must now have well-known electrical properties (delay and loss). The success and quality of the calibration procedure depends largely on the extent to which these properties are accurately known.

At frequencies approaching 1 THz and beyond, the choice of calibration technique is less obvious. Although the TRL method remains more accurate in principle, it becomes increasingly difficult to realize the very short 'line' standard needed to implement a broadband calibration device. (By 'broadband', we refer to a single transmission line standard which will operate successfully over a full waveguide band, approximately a frequency ratio of 1.5:1). The LRL calibration scheme is not generally an attractive solution due to the need for accurate prior knowledge of the first line standard's propagation characteristics. For these reasons, some manufacturers have favored a return to SOLT techniques for VNA calibration at THz frequencies. In waveguide, the open-circuit standard is usually substituted by an offset short-circuit. Detailed reviews of the performance of numerous VNA calibration techniques at THz frequencies can be found in [25, 26]. An alternative solution to this problem is to apply a TRL calibration technique and accept a reduction in the useful bandwidth of the 'line' standard [27]. Successful TRL calibration between 750 GHz and 1.1 THz has been demonstrated using this approach [28]. Other approaches based on measuring multiple lines combined with statistical methods have also been successfully used [29, 30].

VNA measurements at frequencies approaching 1 THz, are subject to a range of additional complicating factors. These are all essentially related to the diminishing physical size of the waveguides used to realize the measurement ports. The most conspicuous complication concerns the lack of repeatability in the waveguide interfaces which has a detrimental effect on both the calibration process and the subsequent measurements. Poor repeatability introduces a significant component of random error in the measurement. Recent studies have shown that this can be a dominant source of error in the measurement [31-33].

2.4 Verification and Traceability

Two important concepts which concern all metrology endeavors are verification and traceability. Verification refers to the measurement of a DUT for which the expected results are well-known, either by prior measurement or prediction from first principles. For VNA-based metrology at millimeter-wave and THz frequencies, the most commonly used verification devices are flush short-circuits and short lengths of transmission line (i.e. waveguide). These are both relatively straightforward to obtain and the electrical properties may be predicted with a high degree of confidence. An additional approach to verification has been reported which uses a 'cross-connected' waveguide to form a predictable attenuation [34, 35].

The uncertainty associated with a measurement is an expression of the confidence the metrologist may have in the measurement. Uncertainties are normally stated in statistical terms, where the true value of the measured quantity is expected to lie within a specified number of standard deviations from the measured value. For residual systematic errors and uncorrected random errors, the dispersion is either assumed to follow a normal (Gaussian) distribution or it is mathematically converted to approximate such a distribution, to enable a combined uncertainty to be expressed [36].

Traceability is the means by which the overall uncertainty associated with a measurement result is assured through a continuous chain of certified calibrations, originating with a national standards laboratory and ultimately, the base quantities which underpin the SI system of units. To establish the traceability, for any given measurement, it is necessary to use one or more reference standards in the calibration procedure which can be linked in some meaningful way to these base quantities. During the past decade, considerable progress has been made toward establishing traceability for VNA measurements above 100 GHz, for example [37-39]. Recently, these activities have extended to cover VNA metrology up to 1.1 THz [28, 40]. The uncertainty in the electrical properties (scattering parameters) of the reference standards is typically determined from dimensional measurements on a section of precision waveguide, and then computing the electrical behavior through electro-magnetic simulations. This enables measurements obtained from a VNA calibrated with these standards to have a meaningful uncertainty.

2.5 THz VNAs: State-of-the-art

Presently, commercial millimeter-wave and THz VNAs operate at frequencies up to 1.1 THz [41]. However, development of the frequency multipliers and other components necessary for implementing VNA extender heads for use at even higher frequencies remains an active field, with one manufacturer recently announcing a 1.5 THz module. VNAs operating at frequencies up to 1 THz produce a typical stimulus signal power in the region of 1 μW. By applying narrowband detection of the down-converted (IF) measurement signals, a typical dynamic range of around 60 dB is achieved under standard laboratory conditions. The frequency accuracy of VNA signal sources based on frequency-multiplying is generally around 1 ppm. This equates to a frequency accuracy of around ±1 MHz at 1 THz. This may be improved significantly by locking the VNA's synthesized frequency sources to an external frequency reference oscillator (linked to a primary frequency standard). In addition, both the transmitter and receiver oscillators are locked to the same reference oscillator, which allows narrowband filtering to be achieved even when there is a drift in the signal frequency. The frequency precision (i.e. 'linewidth') is ordinarily much better than the nominal accuracy implies, owing to the narrowband IF detection.

Figs. 4, 5 and 6 show some typical results of measurements made using a VNA operating in the WM-250 waveguide band [6] (operating from 750 GHz to 1.1 THz). These are reflection and transmission measurements (i.e. *S*-parameter measurements) made on a precision, well-matched,

waveguide line of nominal length 25 mm. Fig. 4 shows a measurement of the linear magnitude of the voltage reflection coefficients (i.e. S_{11} and S_{22}), for the waveguide line, across the full bandwidth of this waveguide size. At most frequencies, the linear magnitude of the reflection coefficient is less than 0.1 (i.e. equivalent to a return loss of better than 20 dB).
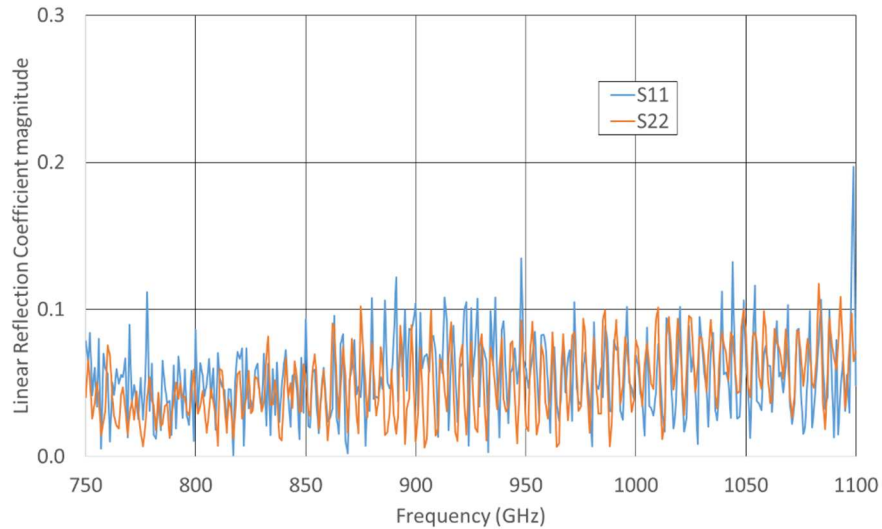
Fig. 4. VNA measurements of the magnitude of the reflection coefficients, S_{11} and S_{22}, for a 25 mm well-matched precision WM-250 waveguide line

Fig. 5 shows the measured attenuation (or, equivalently, transmission coefficients, S_{12} and S_{21}), across the full waveguide bandwidth, for the same 25 mm waveguide line. This shows that the loss in the line is less than 3 dB across most of the band. The average attenuation is approximately 2.5 dB, which is equivalent to an attenuation constant of approximately 1 dB/cm. This shows good agreement with calculated values of attenuation constant given in [6], which range from 0.8 dB/cm, at the maximum frequency (1.1 THz), to 1.3 dB/cm at the minimum frequency (750 GHz) for this waveguide band.
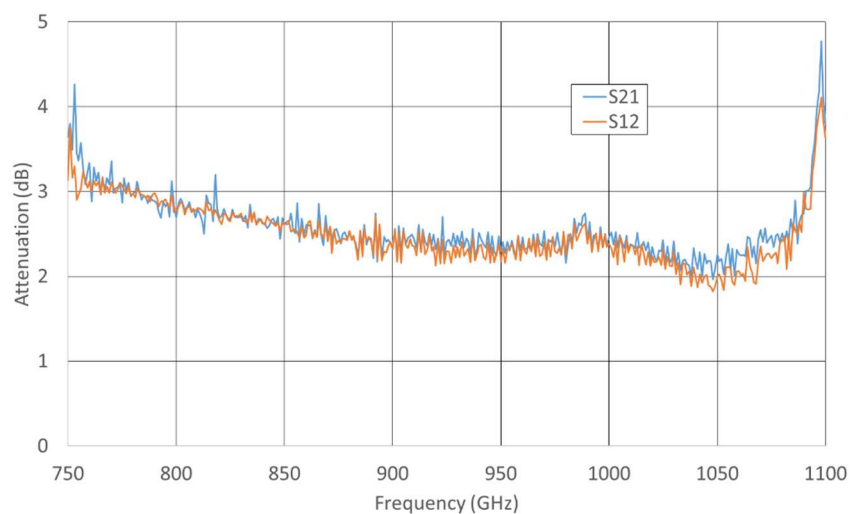

Fig. 5. VNA measurements of attenuation (i.e. transmission coefficients, S_{12} and S_{21}) for the same waveguide line measured in Fig. 4

Finally, Fig. 6 shows the measured transmission phase (S_{12} and S_{21}) for the same 25 mm waveguide line. Only values over a restricted frequency region (i.e. from 1.05 THz to 1.1 THz) are shown here. Values across the rest of the waveguide band show similar behavior – i.e. a characteristic saw-tooth pattern due to the length of the line being equivalent to many waveguide wavelengths, at these frequencies. The small difference between the measured phases of S_{12} and S_{21} (of approximately 15°), at each frequency, is likely due to minor errors in the measurements – perhaps due to incorrect assumptions concerning forward and reverse signal path lengths, or, instability in the amplitude and phase in the RF, LO and IF cables between the VNA and the extender heads.
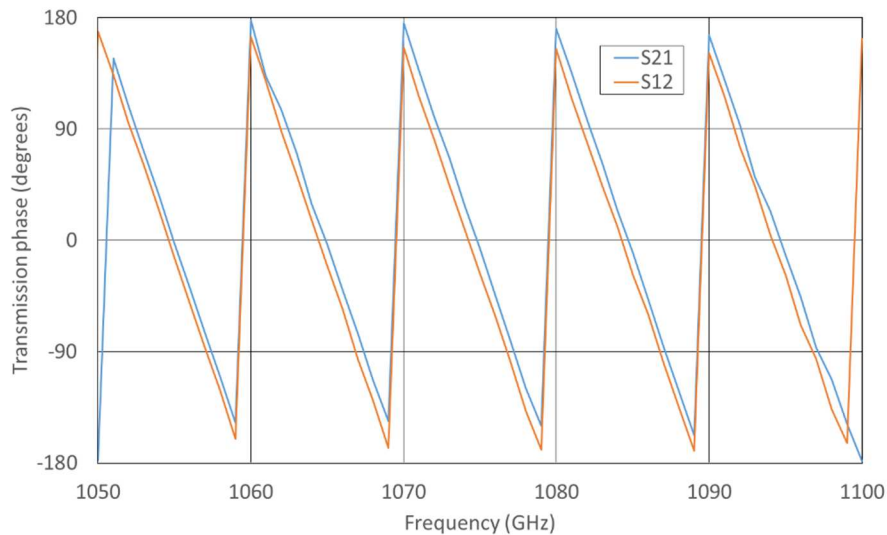

Fig. 6. VNA measurements of transmission phases, for S_{12} and S_{21}, for the same waveguide line measured in Figs. 4 and 5

3. Terahertz Time-Domain Spectrometers

TDS is similar to VNA in that both incorporate coherent detection that measures directly the field amplitude and phase of the electromagnetic wave. As a consequence, both provide a straightforward and unambiguous determination of attenuation and phase shift resulting from beam interaction with the sample studied. However, unlike a VNA, which sweeps through its frequency band, recording data at each frequency consecutively, pulsed TDS acquires broadband data in time-domain. In recent years, THz TDS metrology has attracted considerable attention, indicating the maturation of the field and reflecting the strong growth and diversity of applications.

3.1 THz TDS operation

The full spectral bandwidth produced by a pulsed THz emitter as used by TDS is contained in a single-cycle THz pulse. In order to perform coherent detection, TDS operates in a "closed-loop" pump-probe configuration whereby the pump and probe beams are derived from the same laser source, and the detector is gated by the combined presence of THz and probe pulses. This makes possible the high signal-to-noise ratio and dynamic range of these systems [42].

Pulsed THz TDS systems are activated by ultrafast lasers with a pulse length typically shorter than 100 fs. In the pump-probe configuration, the laser beam is split into two, with the majority of the power

being used to generate THz, and a minor fraction diverted for use as the probe, as depicted schematically in Fig. 7. The THz and probe pulses are re-combined on the detector, arranged so as to overlap temporally as well as spatially. The detector signal is proportional to the product of probe intensity and the THz field. The probe pulse length is that of the pump laser, and is of the order of 10 fs to 100 fs; whereas the THz pulse length one or two orders of magnitude longer, typically 1 ps to 2 ps. The overlap time point can be varied by employing adjustable delay between probe and THz beams, thus causing the probe to sweep through the THz pulse, as depicted in Fig. 8. At each delay position, the detected signal represents the THz field whilst the relative delay corresponds to its phase: thus both field amplitude and phase are directly probed and recorded.
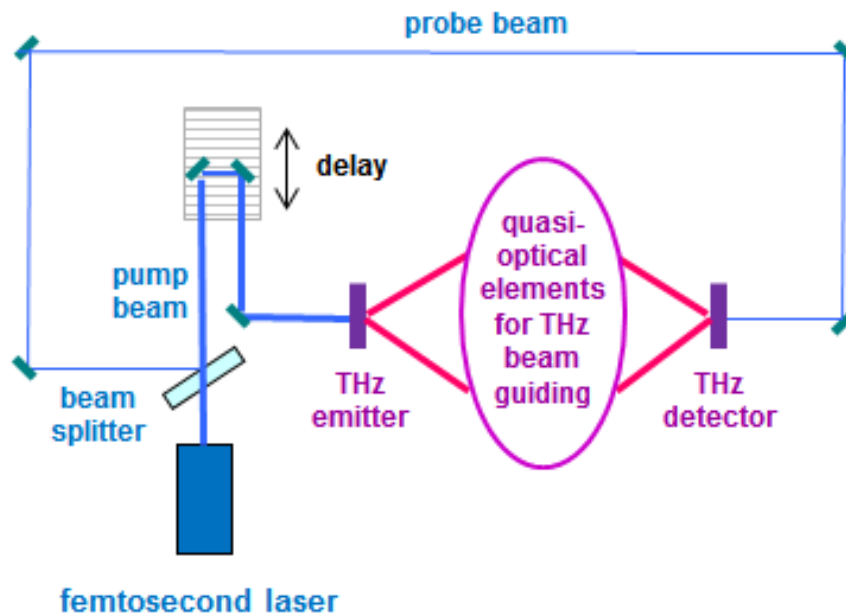

Fig. 7. Schematic drawing of a THz time-domain spectrometer.

THz TDS emitters are primarily of two types: photoconductive (Austen switch) or optical rectification (a nonlinear optical process) [43]. THz TDS detectors are also of two types: photoconductive or electro-optic [43]. Any combination of emitter and detector type may be employed, with some variations in the resulting performance; commercial systems predominantly use photoconductive emitters and detectors. All THz TDS emitters produce pulses whose temporal profiles, depicted in Fig. 8, are broadly similar, and whose duration is proportional to the pulse length of the pump laser. The spectral profile, obtained via Fourier Transform, has the form shown in Fig. 8 (inset). This spectral profile has two salient features which have a crucial bearing on all aspects of THz TDS measurements: the amplitude decreases steeply with frequency; and the slope of the fall is inversely related to the duration of the temporal oscillation. Many of the metrological issues pertaining to THz TDS arise from this aspect of its operation, namely that data is acquired in time-domain whereas the derived optical properties of the sample being studied are calculated in frequency-domain.

3.2 THz TDS operational specifications

Some of the core operational specifications of a spectroscopy system are its spectral bandwidth and frequency resolution, and its dynamic range (DR) and signal-to-noise ratio (SNR). For a THz TDS, the

SNR and DR may be evaluated either from the time-domain data or from the calculated frequency-domain spectrum, where they produce very different results with no simple analytical relationship between the two sets of values [43]. Furthermore, the achievable frequency resolution is limited by the DR in time-domain, whilst the spectral bandwidth is determined by the DR in frequency-domain.
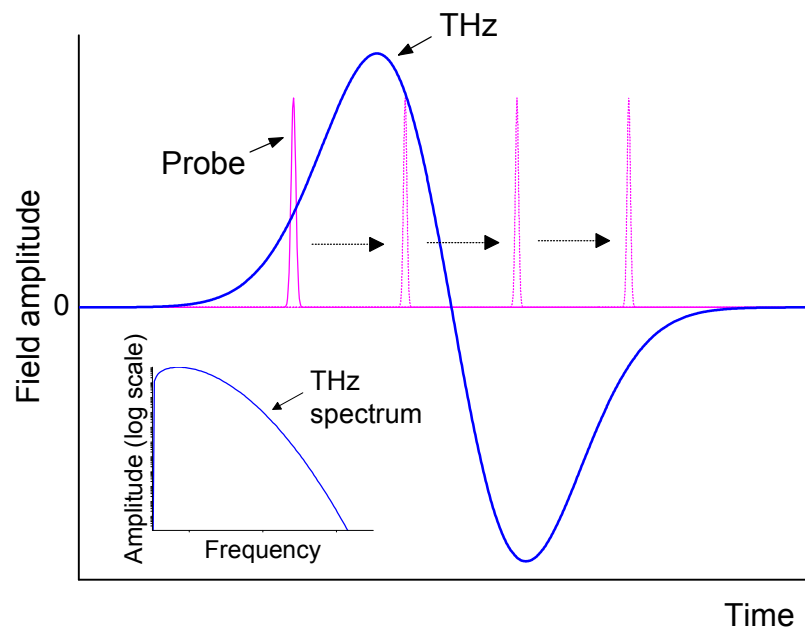

Fig. 8. Schematic depiction of THz TDS operation: probe pulse sweeping and recording the amplitude and phase of the THz pulse (model data). Inset: Frequency spectrum of the time-domain signal obtained via Fourier Transform.

Fig. 9a shows part of a typical time-domain trace of a THz pulse. Also plotted are the dynamic range and the SNR of this data. It is seen that the DR is largest where the signal is strongest; indeed, it has been observed empirically to be roughly proportional to the absolute value of the signal amplitude. In contrast, the SNR fluctuates strongly and irregularly from point to point, to the extent that it provides no meaningful information as to the system performance.

The spectral amplitude profile derived from the time-domain data and its DR and SNR are shown in Fig. 9b. Because the dynamic range is defined as the ratio of amplitude at a particular frequency to the noise floor, the DR spectral profile is similar to that of amplitude. The SNR, on the other hand, is notably flat over a large part of the spectrum; then drops with the falling amplitude. It is a widely accepted custom to quote the maximum value of the dynamic range in frequency-domain as the DR of a TDS system. This approach is justifiable to a degree, because the great majority of TDS systems produce similar spectral profiles, and the frequency dependence of the DR follows that of the source spectrum.

An important consequence of the typical values of the SNR and DR in frequency-domain is that the large DR allows the examination of strongly attenuating samples, while the much lower SNR limits the accuracy and amplitude resolution of these measurements. Similarly, in time-domain, the high DR at the peak maximum makes it possible to detect loss variations in strongly absorbing materials and artefacts. As mentioned above, the frequency resolution and bandwidth of a TDS are governed by its DR in time-domain and frequency-domain respectively.
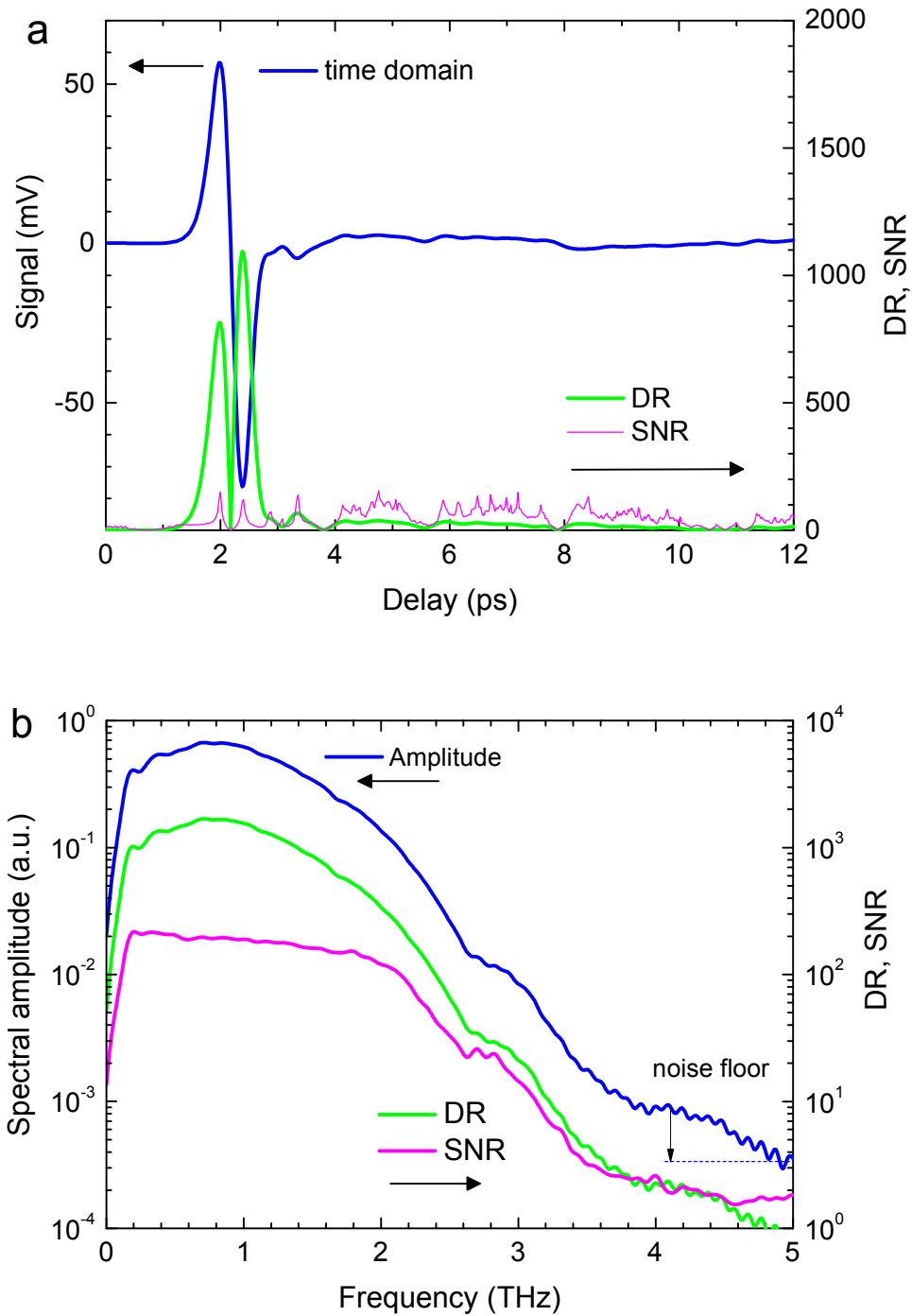
Fig. 9. a) Part of a THz pulse time-domain data set and its dynamic range and SNR. b) Spectral profile of the THz pulse obtained from the data in (a) and its dynamic range and SNR.

In a pulsed THz TDS the frequency resolution is set by the frequency interval of the spectral data and is ultimately limited by the system DR. As the outcome of Fourier Transform, this data frequency interval is given by $c/2L$, where c is the speed of light and L is the length of the delay sweep. In a noise-free system with unlimited available delay, the maximum resolution of a pulsed TDS would be equal to the repetition rate of the pump laser. However, in the presence of noise the achievable frequency interval is much larger, because the signal amplitude, and its DR, diminishes with increasing delay from

the main pulse, eventually approaching unity. From that point onwards, scanning to longer delays adds no further data, since the signal is drowned in noise, therefore limiting the usable delay. A study of the dependence of the TDS frequency resolution on noise concluded that in a typical system the maximum achievable resolution is of the order of 1 GHz [44]. In common experimental practice, it is advisable to limit the delay scan length to the region where DR > 2.

One of the most important papers dealing with the dynamic range of THz TDS systems and its implications on the bandwidth was published by Jepsen and Fischer [45]. They pointed out that the maximum absorption coefficient α_{max} that is measurable in transmission is determined by the DR via the relationship:

$$\alpha_{max}d = 2\ln\left[\frac{E_{max}}{E_{min}}\frac{4n}{(n+1)^2}\right] = 2\ln\left[DR\frac{4n}{(n+1)^2}\right] \tag{1}$$

where d is the sample thickness and n its refractive index. E_{max} is the reference field, and E_{min} is the noise floor. That is because the absorption coefficient is calculated from the ratio of the reference and sample spectra using an equation of the form of Eq. 1. The minimum measurable sample spectrum must remain above the noise floor, therefore determining the maximum measurable absorption. Since the dynamic range of a TDS-produced spectrum falls with frequency (Fig 9b), while absorption typically increases, Eq. 1 sets an upper bound on the effective measurement bandwidth. Fig. 10 is an experimental demonstration of Eq. 1. The measured absorption coefficients of two different material samples are plotted together with respective α_{max} calculated from Eq. 1. It is seen that at frequencies above the intersection of $\alpha = \alpha_{max}$ the absorption spectrum becomes very noisy and decreases in line with the α_{max} curve. In interpreting absorption data, this is a visual indicator that the dynamic range of the system has been exceeded and that the data from that point onwards are no longer valid or meaningful. Note also that in Eq. 1 the maximum measurable absorption is inversely proportional to the sample thickness, affecting the selection of optimum sample parameters.

Because of the effect of noise in limiting the frequency resolution and the measurement bandwidth of a THz TDS, sources of random noise are critically important to its operation. Mechanical sources of amplitude noise include vibrations, air currents in the beam paths, particulates in the air along the beam paths, and thermal deformations. Amplitude noise may also arise from pulse-to-pulse variations in the pump laser intensity. However, even when all sources of electronic and mechanical noise have been minimised, the residual amplitude noise in TDS systems tends to be of the order of 1% of signal intensity. This was seen to be the case by Hübers et al. [42] who have tested different TDS systems, incidentally confirming that amplitude noise is proportional to the absolute value of amplitude. Laser amplitude fluctuations, beam pointing deflections, and detector noise were all considered as possible noise sources, but were found to be too small to account for the observed noise levels [42, 46, 47]. Moreover, it was seen that the random errors in amplitude and phase spectra of a TDS are independent of each other, and therefore are unlikely to be attributable to a common cause. Identifying the sources of amplitude noise and reducing it is one of the challenges in TDS design.
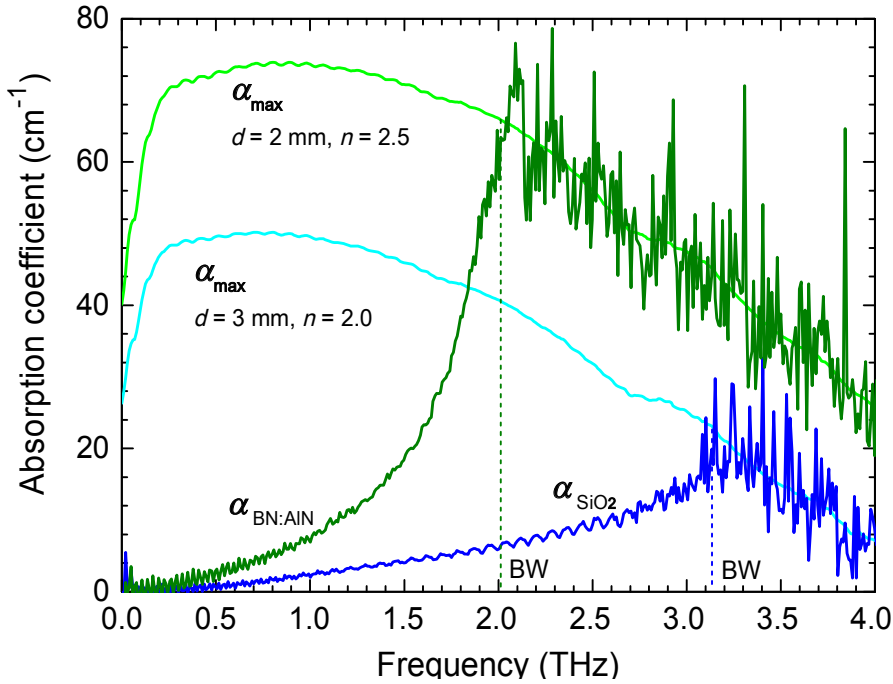
Fig. 10. Experimental demonstration of Eq. 1. α_{max} is calculated for two samples: fused silica (SiO$_2$, d = 3 mm, n = 2.0), and ceramic BIN77 (50BN:50AlN, d = 2 mm, n = 2.5); α_{max} is larger for the thinner sample. It is seen that absorption cannot be measured beyond α_{max}, and that this limits the available frequency bandwidth.

Random delay positioning errors can be an important source of both amplitude and phase noise. In particular, delay jitter has been found to raise the noise floor in frequency domain [48, 49], thus affecting the bandwidth. In contrast, systematic positioning error, i.e. incorrect registration of the positional scale, produces an error in the frequency scale via Fourier Transform, and can be identified and rectified by frequency calibration (see below). Although TDS systems such as ASOPS (asynchronous optical sampling) do not employ mechanical delay, they may experience similar issues of random and systematic phase noise due to errors in laser synchronisation and/or drift in the pulse repetition rates.

3.3 Optical parameter extraction

Because the main use of TDS is in material characterization, a large amount of literature has been devoted to the subject of parameter extraction, i.e. to calculating the optical parameters of the materials studied from their THz transmission spectra. In common with other spectrometers, TDS measurements require comparison between the data recorded with the sample placed in the beam path and reference data recorded with the sample removed. First measurements of dielectric constants of materials were demonstrated soon after the invention of TDS by Grishkowsky et al. [50]; thereafter many refinements to the calculation procedures were proposed [51-54]. Particular issues arising in the case of thin (sub-wavelength) samples were also considered [55, 56]; as well as the optimal sample thickness [57]. Uncertainties in the parameter calculations have been analysed in detail, and computational approaches developed to quantify these and to reduce them, where possible [58-60]. Systematic errors arising from beam defocusing caused by placing optically thick samples at the focal plane of the THz beam have been investigated and shown to be significant [61, 62], confirming that a collimated beam should be used for high-accuracy measurements.

A comprehensive analysis of all sources of uncertainty in the derived THz optical parameters was presented by Withayachumnankul et al. [63]. Random (R) and systematic (S) errors arising from both system operation and calculation procedures were considered and their magnitudes evaluated, including: electronic and optical noise (R and S), interface reflections in the sample (S), sample alignment in the THz beam (R and S), sample thickness measurement (R and S), and calculation errors (e.g. approximations, rounding (S)). The conclusion was that the main contributing factors to parameter uncertainty are signal noise and the uncertainty in sample thickness.

3.4 Calibration

THz TDS systems face two issues of calibration: frequency; and linearity of response. In contrast, the absolute value of the THz power generated by the emitter has no direct bearing on the measurement, and is only required to remain constant in the course of data acquisition. With respect to frequency calibration, THz TDS may be considered as having an operational advantage in that calibrating the frequency scale also provides verification of the phase data. This is because both frequency and phase are derived from the time-domain delay via Fourier Transform, so that an accurate frequency scale also guarantees accurate phase measurement, and consequently parameters derived from it (e.g. refractive index, or sample thickness). In order for the measured spectral profile to be accurately defined, the amplitude scale must be known to be linear. As a "closed-loop" system, THz TDS differs from other types of spectrometer in that its source and detector are both activated by the same laser pulse and form an integral system. As a result, the linearity of its amplitude response depends on multiple factors of signal-probe interaction, including individual alignment of terahertz and probe beams, beam overlap, spatial beam profiles, and temporal pulse shapes, thus necessitating linearity calibration to ensure correct instrument performance. In recent years calibration techniques and standards for THz TDS have been attracting increasing attention; an overview of this work and its current status was presented by Shimada et al. in [64].

Frequency calibration can be accomplished using an absorption cell containing a suitable gas [43, 65]. This would preferably be a gas having a linear molecular structure whose absorption spectrum consists of a regular comb of lines with a characteristic amplitude envelope. Such gases offer the advantage of well-known line frequencies and narrow linewidths (a few GHz). However, gas cells are relatively bulky and inconvenient; and moreover pose safety hazards since suitable gases are almost invariably toxic (e.g. CO). For those reasons, an etalon is preferable for most applications [64-66]. A Fabry-Perot etalon as a frequency calibration artefact also has the important advantage in that it produces a regular frequency comb across the whole operating band of the THz TDS; and moreover, that its frequency spacing or free spectral range (FSR) can be chosen to suit the desired application. The two drawbacks of an etalon are that its FSR must be independently determined, and that its loss peaks are relatively broad (10-100 GHz, depending on the finesse).

A frequency calibration etalon must fulfil two requirements: its dispersion must be negligible, i.e. the frequency spacing must be constant throughout the THz measurement band; and its absorption loss must also be negligible. A high-resistivity silicon wafer may be used as a low finesse etalon [43, 65]; alternatively, a high-finesse air-gap etalon may be fabricated [64, 66]. The simplest method of frequency calibration using an etalon is to record the frequencies of the peaks and troughs in its transmission spectrum and to compare them with their expected values [43, 65], where $FSR = c/2nd$ (n is the refractive index of the etalon material, and d is its thickness). The difference between the measured and expected frequencies for each peak/trough can then be plotted as a function of its expected

frequency, as shown in Fig. 11, revealing any systematic frequency errors as well as digitizing errors and noise.

Deng et al. [67] demonstrated a technique for in-line calibration of a TDS using a combination of both a gas cell and an etalon that enables the frequency scale of every set of time-domain data to be verified in the process of data acquisition. First, a CO gas cell is used to determine accurately the FSR of the etalon; thereafter, each set of time data is adjusted so as to reproduce the correct FSR in the frequency domain. This makes it possible to counteract jitter in the delay line.
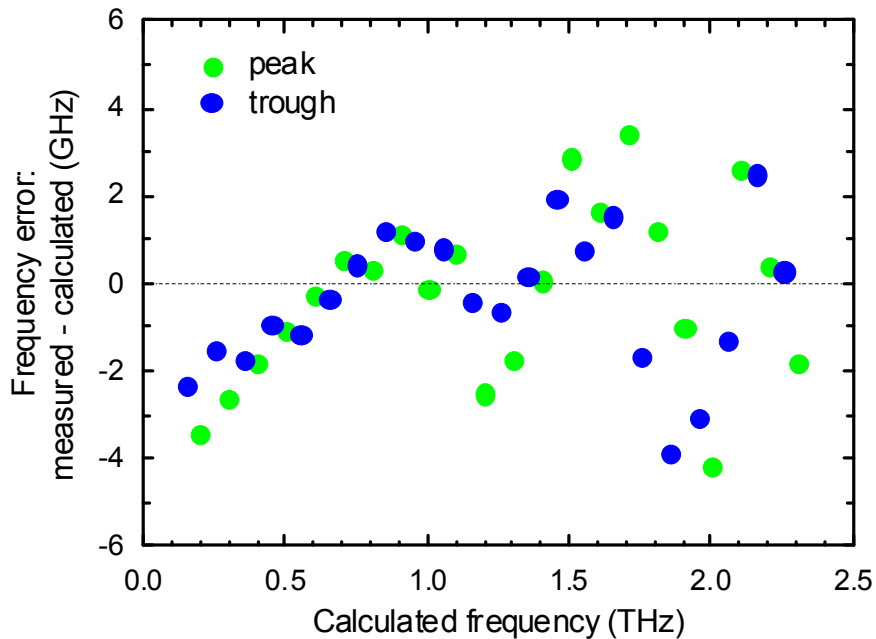

Fig. 11. Differences between the measured and expected peak/trough frequencies using a Si wafer etalon with a free spectral range of 100 GHz.

A calibration artefact for testing amplitude linearity of a THz TDS system must have two attributes: attenuation that is well defined and constant across the operation band; and the ability to produce multiple accurate attenuation steps spanning the dynamic range of the system. A solution was demonstrated using a stack of "loss elements" in the form of high-resistivity silicon plates [43, 65]. Due to its negligible absorption and dispersion in the terahertz band, transmission loss of high-resistivity silicon is frequency-independent and due solely to Fresnel reflections. The loss produced by a stack of plates separated by air gaps is multiplicative, to the power equal to the number of plates in the stack. Fig. 12 shows an example of linearity calibration using silicon plates, where the expected slope for linear behaviour is 0.7. It is seen that the system is close to linear at frequencies where the DR is large (see Fig. 9b); and that it deviates from linearity where the DR is reduced (at 3 THz).

Silicon plates are widely available and convenient to use. However, due to their large optical thickness, when they are placed in a focused beam they cause significant beam defocusing which results in a systematic error, making them unsuitable for calibrating systems that use focused beams. Moreover, the stack is relatively bulky, and cannot be easily accommodated in the sample compartment of many commercial systems. An alternative approach was developed by Iida et al. using thin metallized-film attenuators, which can be employed in combinations to produce multiple attenuation stages [64, 68]. The linearity of a THz TDS instrument should be verified as a routine calibration step, in view of the many possible causes of nonlinearities in the system [64, 65, 68].
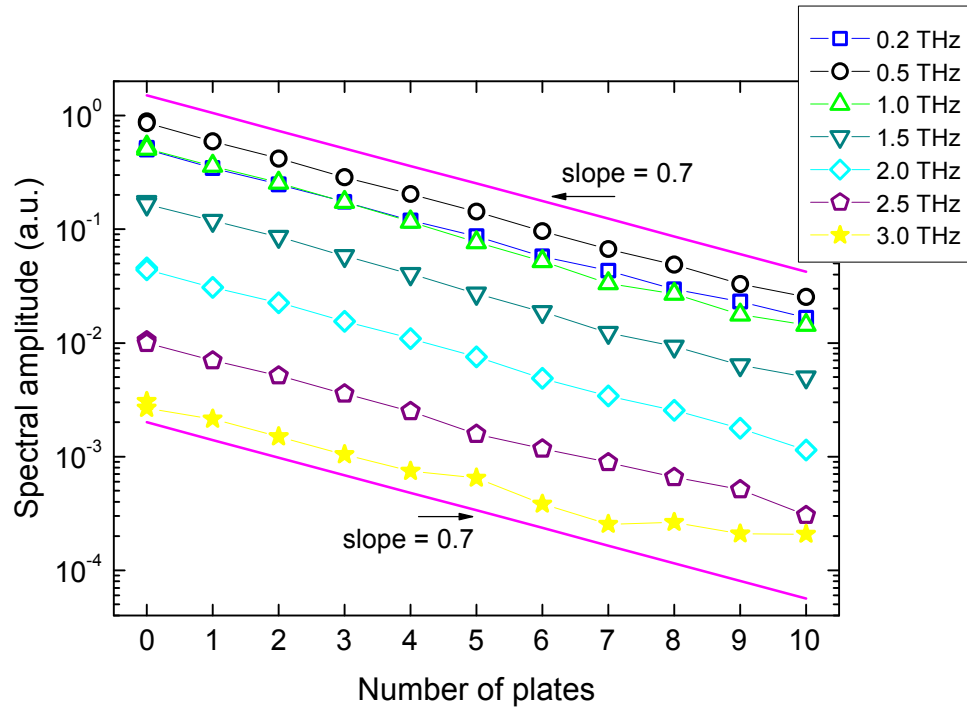
16

Fig. 12. Linearity test of a THz TDS using a stack of high-resistivity silicon plates. The expected amplitude slope for linear behaviour is 0.7.

3.5 TDS intercomparison

In the light of the scope and detail of published work addressing various aspects of THz TDS metrology – i.e. noise and error analysis, parameter extraction, and calibration – it may be argued that a sufficient foundation exists for establishing a standard methodology for measuring and calculating THz optical parameters and their uncertainties. However, a mechanism for adopting and disseminating such standards is still lacking in the THz community. In order to draw attention to the diversity of practice and to establish how it affects the measurement outcomes, the National Physical Laboratory in the UK is currently running an international THz TDS measurement comparison study, due to conclude during 2016 [69]. An international group of THz TDS practitioners have been recruited to participate, including national measurement institutes, academia, and THz system manufacturers. A set of standard material samples have been prepared, and measurements of their refractive indices and absorption coefficients reported by participants will be collated and analyzed. A set of 5 materials widely used in THz optics and measurements was chosen, representing a range of dielectric properties: high-resistivity silicon, *z*-cut quartz, silica glass, high-density polyethylene (HDPE), and a lactose monohydrate pressed-powder pellet. An additional benefit of this study will be to establish accurate values of the THz optical constants of these materials.

Fig. 13 shows some of the initial results (from 5 participants) and the significant variations between them. This demonstrates the need to arrive at a standard measurement methodology and to adopt a set of standard test materials whose THz optical properties are accurately known.
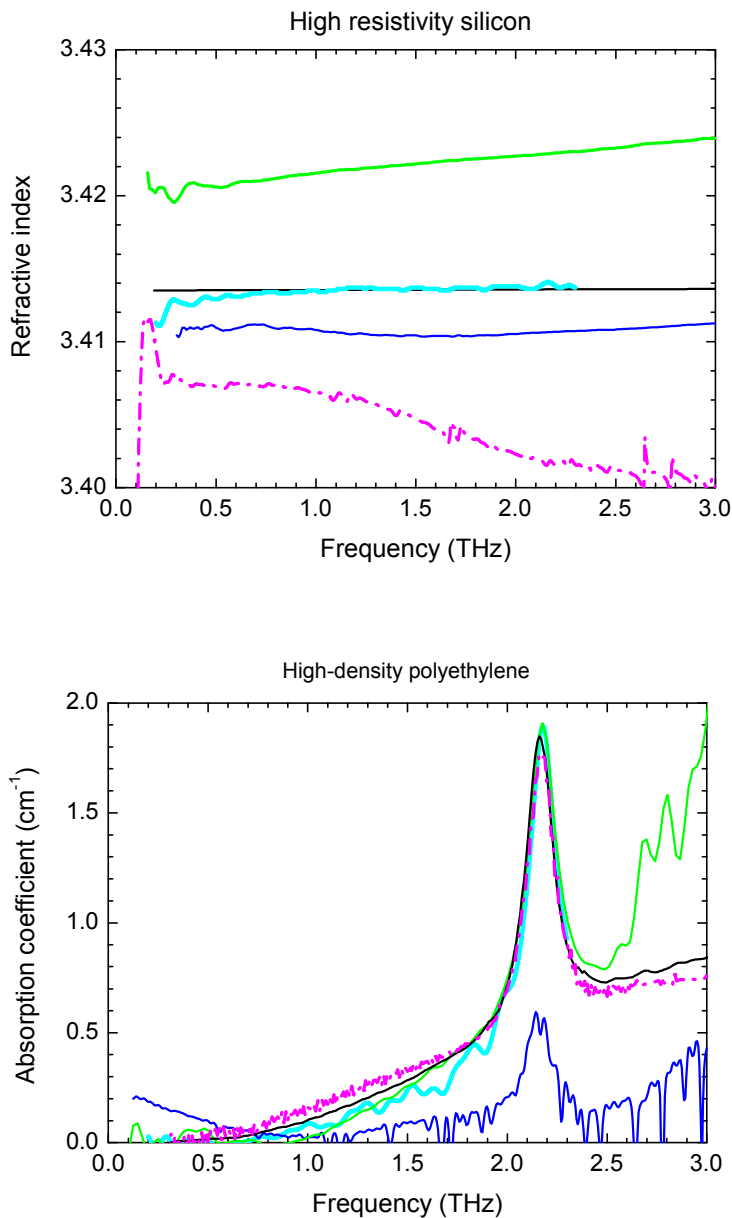
High resistivity silicon

High-density polyethylene

Fig. 13. Initial results from 5 different participants in the THz TDS intercomparison study.

3.6 TDS-VNA intercomparison

As the operational bandwidth of VNAs has expanded and instruments operating above 1 THz have become more common, VNAs have begun to be used for material characterisation, where they are configured for free-space measurements similar to TDS (Fig. 14) [70, 71]. This overlap in applications makes it particularly important to be able to establish and demonstrate the equivalence of measurement results obtained by TDS and VNA. A rigorous metrological analysis of a free-space VNA and its comparison with a TDS was presented by Tosaka et al [72]. A critical issue in such measurements is the mutual alignment of the horns, which is very difficult to achieve and verify; and the effects on beam propagation and alignment caused by the insertion of samples in the beam path. An alternative approach to VNA-TDS intercomparison of measurements employs the VNA in its customary waveguide-based

configuration, rather than in free-space [73]. This is accomplished by using a deformable test material (petroleum jelly) that can fill either a hollow metallic waveguide for a VNA or a transmission cell for a TDS. Such VNA-TDS comparison studies have found satisfactory agreement between the two instrumental platforms. More detailed work is needed to establish a full inter-operability of VNA and TDS and their associated measurement domains.
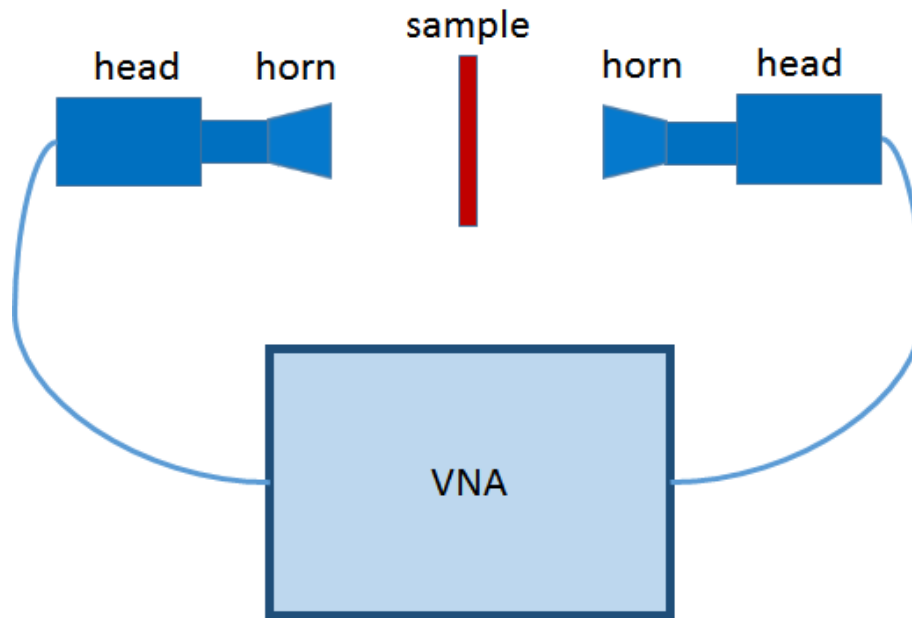

Fig. 14. Schematic drawing of a free-space VNA setup for material measurements.

4. Electro-optic Sampling

EOS is a specialized type of TDS used as a primary standard for voltage waveform measurements. In contrast to TDS, which operates in free-space, the THz signals are guided on a coplanar transmission line, typically on a Gallium Arsenide or Lithium Tantalate substrate. The potential of this technique was quickly recognised by National Measurement Institutes (NMI) [74, 75] as a physics-based solution to calibrate traceably the impulse response, rather than the bandwidth, of instruments such as sampling oscilloscopes. The highest frequency in the coplanar waveguides is typically less than 1 THz [76], see Fig. 15, depending on the architecture and electrical impulse. At present there is no need for a multi-THz bandwidth as the electrical pulse is coupled into a coaxial geometry to match the sampling oscilloscope input connector. Although fewer than five primary standard systems have been reported worldwide their fan-out is large, providing traceability for the world-wide oscilloscope market. More recently these systems have provided traceability for the phase-standards that underpin Nonlinear Vector Network Analyzers (NVNA) and have been used to complement VNA systems by measuring integrated circuits [77] and THz antenna patterns [78].
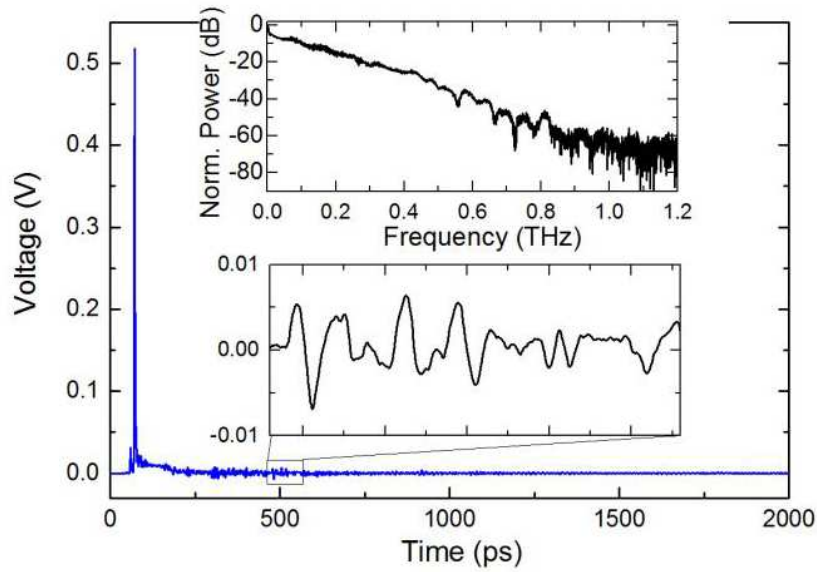
Fig. 15. Voltage pulse for EOS measured over a time window of 2 ns after a propagation distance of ~2 mm on a 4 mm long coplanar waveguide. The upper and lower insets display the power spectrum of the voltage pulse and a magnified waveform detail [75] reproduced courtesy of Dr M Bieler.

Fig. 16 shows a schematic diagram of an EOS set-up. As in TDS, the beam from a femtosecond laser is split into pump and probe. As in TDS, the pump beam activates a THz emitter. In EOS, photoconductive switches (with rise-times of between 1 ps and 2 ps) or photodiodes (with rise-times of between 3 ps and 5 ps) are commonly used to generate the THz pulse. The THz signal then propagates down a coplanar waveguide (or another type of suitable circuit structure), where it encounters and interacts with the probe beam or the EOS probe head both of which operate similarly to electro-optic detection in TDS. An important advantage of EOS in detecting high-frequency fields in circuits and devices – and one of the main rationales for its use – is its non-contact nature.
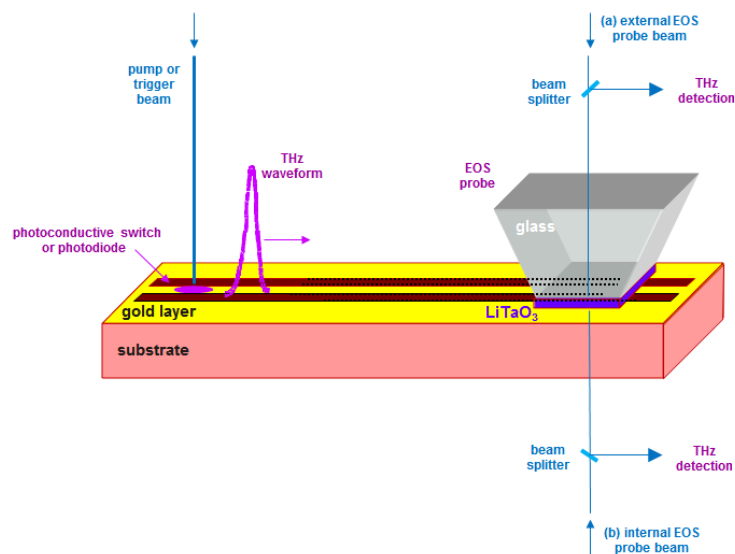

Fig. 16. Schematic drawing of EOS. (a) Internal EOS uses substrate material for EO detection (GaAs or LiTaO₃); (b) external EOS employs a probe head with a layer of EO material (LiTaO₃). Most systems use either External (a) or Internal (b) EOS but not both.

The EOS can be implemented either by using a probe head [74, 79] or by direct interaction of the probe beam with the substrate (Fig. 16) [80]. Gallium Arsenide (GaAs) or Lithium Tantalate (LiTaO$_3$) are most often employed as the electro-optic material. Due to their high permittivity, both of these electro-optic materials (and others) cause significant distortion of the electric field [81]. Using a small probe head is advantageous because of its small size and therefore reduced effect on the measured field [80].

Error-correction and uncertainties in EOS have received considerable attention within the NMI community [82, 83], because the waveform needs to be evaluated at the plane of the DUT, rather than simply measured at a point on the coplanar waveguide substrate. For example, in a VNA, the forward and reverse travelling electrical waves are often separated using directional-couplers in the test-set, but in an EOS both components contribute to the measured temporal field. Workers at PTB in Germany [83] have measured the field at two points on the transmission line, making it possible to separate the forward and reverse waveforms. This work demonstrated that corrections can be applied successfully to determine the impedance-match corrected response of the instrument. As the pulse response shows a gradual degradation the result is less prone to truncation artifacts [82]. These approaches also show strong links to developments made with THz VNAs [83].

The future measurement challenges for EOS include extending the bandwidth to 1.5 THz and above (to complement the developing state-of-the-art for VNA operating frequencies), improving resolution to separate forward and reverse travelling waves (optical VNA) and to reduce the invasive field distortion.

5. Concluding remarks

The broad area of THz measurements is set to continue its rapid expansion, utilizing all types of instrumentation platforms, free-space and waveguide-based [84]. The number and diversity of THz applications is likewise growing. Even more importantly, THz technologies are transitioning from academic research to industrial applications, with widespread uptake being envisaged in the course of the next decade. Robust metrological underpinning is necessary to support both scientific research and industrial applications; moreover, equipment manufacturers demand, and end-users benefit from, established standards and calibration services.

Several issues require to be addressed in particular. For TDS these are: establishment of standardised measurement, calibration, and data analysis procedures. For VNA, engineering solutions are needed for high-precision waveguides and interconnects. In addition to these, inter-operability and inter-comparability must be achieved between TDS and VNA for characterization of material properties, and between EOS and VNA for measurements on circuits and devices.

The ultimate goal is to establish a robust framework of metrological traceability to the International System of units (SI) for the portfolio of measurands (i.e. for physical quantities that need to be measured) that are, and will be, needed to underpin scientific and technological developments in the years to come. This framework will ensure the reliability and equivalence of all measurements made at terahertz frequencies. This is a pre-requisite for effective science, trade and industry that exploits the terahertz region of the electromagnetic spectrum.

References

[1] K. Kurokawa, "An Introduction to the Theory of Microwave Circuits", Academic Press, New York and London, 1969.

[2] R. B. Marks and D. F. Williams, "A General Waveguide Circuit Theory", Journal of Research of the National Institute of Standards and Technology, vol. 97, pp 533-562, 1992.

[3] MIL-DTL-85/3C, "Waveguide, Rigid, Rectangular (Millimeter Wavelength)", February 2002.

[4] H. Li, A. R. Kerr, J. L. Hesler, H. Xu, R. M. Weikle, "A Ring-Centered Waveguide Flange for Millimeter- and Submillimeter-wave Applications", IEEE MTT-S International Microwave Symposium, Anaheim, CA, USA, pp. 604–607, May 2010.

[5] M. Horibe and R. Kishikawa, "Performance of new design of waveguide flange for measurements at frequencies from 800 GHz to 1.05 THz", 79th ARFTG Microwave Measurement Conference, Montreal, CAN, June 2012

[6] IEEE Std 1785.1-2012, "IEEE Standard for Rectangular Metallic Waveguides and Their Interfaces for Frequencies of 110 GHz and Above—Part 1: Frequency Bands and Waveguide Dimensions", 2013.

[7] IEEE Std 1785.3-2016, "IEEE Standard for Rectangular Metallic Waveguides and Their Interfaces for Frequencies of 110 GHz and Above—Part 2: Waveguide Interfaces," 2016.

[8] P. G. Bartley and S. B. Begley, "A new free-space calibration technique for materials measurement," Instrumentation and Measurement Technology Conference (I2MTC), pp 47–51, 2012.

[9] M. F. Bauwens, N. Alijabbari, A. W. Lichtenberger, N. S. Barker, R. M. Weikle, "A 1.1 THz micromachined on-wafer probe," Microwave Symposium (IMS), 2014 IEEE MTT-S International, 2014.

[10] C. Caglayan, G. C. Trichopoulos, K. Sertel, "Non-Contact Probes for On-Wafer Characterization of Sub-Millimeter-Wave Devices and Integrated Circuits", Microwave Theory and Techniques, IEEE Transactions on, On page(s): 2791 - 2801 Volume: 62, Issue: 11, Nov. 2014.

[11] D. F. Williams, A. C. Young, M. Urteaga "A Prescription for Sub-Millimeter-Wave Transistor Characterization", IEEE Trans THz Sci. and Technol., Vol 3, No 4, pp 433 – 439, Jul. 2013.

[12] A. Maestrini, B. Thomas, H. Wang, C. Jung, J. Treuttel, Y. Jin, G. Chattopadhyay, I. Mehdi, G. Beaudin, "Schottky diode based terahertz frequency multipliers and mixers," C. R. Physique, Vol 11, 2010.

[13] R. E. Collin, "Foundations for Microwave Engineering", McGraw Hill Inc., 1992.

[14] J. L. Hesler, Y. Duan, B. Foley, T. W. Crowe, "THz Vector Network Analyzer Measurements and Calibration", 21st Intl. Symp. on Space Terahertz Technology, Oxford, UK 23-25 April 2010.

[15] F. C. De Lucia, "Noise, detectors, and submillimeter-terahertz system performance in nonambient environments," Journal of the Optical Society of America B (Optical Physics), vol. 21, no. 7, pp. 1273–9, Jul. 2004.

[16] R. G. Clarke, N. M. Ridler, "Metrology for Vector Network Analyzers", Chapter 9 in "*Terahertz Metrology*", ed. M. Naftaly, Artech House, pp 185-249, 2015.

[17] N. M. Ridler, R. G. Clarke, M. J. Salter, A. Wilson, "The Trace is on Measurements: Developing Traceability for S-Parameter Measurements at Millimeter and Submillimeter Wavelengths", IEEE Microwave Magazine, vol. 14, no. 7, pp. 67-74, Nov./Dec. 2013.

[18] OML (Oleson Microwave Labs), "Frequency extension source modules to extend signal capability from 50 to 325 GHz", Microwave Journal, vol. 47, no. 3, pp. 124-134, Mar. 2004.

[19] G. F. Engen, "The six-port reflectometer: An alternative network analyzer," IEEE Trans. Microwave Theory Tech., vol. 25, no. 12, pp. 1075–1080, 1977.

[20] G. Wu, Z. Liu, R. M. Weikle, "A millimeter-wave sampled-line six-port reflectometer at 300GHz," 15th International Conference on Terahertz Electronics, 2007.

[21] P. Goy, M. Gross and J. M. Raimond, "8-1000 GHz vector network analyzer", 15th Int. Conf. on Infrared and Millimeter Waves (IRMMW), Orlando, FL, USA, December 1990.

[22] W. Kruppa and K. F. Sodomsky, "An explicit solution for the scattering parameters of a linear two-port measured with an imperfect test set," IEEE Trans. Microwave Theory Tech., vol. MTT-19, no.1, pp. 122–123, 1971.

[23] G. F. Engen and C. A. Hoer, "Thru-reflect-line: An improved technique for calibrating the dual six-port automatic network analyzer," IEEE Trans. Microwave Theory Tech., vol. 27, no. 12, pp. 987–993, 1979.

[24] C. A. Hoer and G. F. Engen, "On-line accuracy assessment for the dual six-port ANA: extension to non-mating connectors," IEEE Trans. Instrum. Meas. , vol. 36, pp. 524–529, June 1987.

[25] D. F. Williams, "500 GHz - 750 GHz rectangular-waveguide vector-network-analyzer calibrations," IEEE Trans. THz Sci. Technol., Vol. 1, No. 2, pp. 364–377, Nov. 2011.

[26] D. F. Williams, "Comparison of sub-millimeter-wave scattering-parameter calibrations with imperfect electrical ports," IEEE Trans. THz Sci. Technol., Vol. 2, No. 1, pp. 144-152, Jan. 2012.

[27] N. M. Ridler, "Choosing line lengths for calibrating waveguide vector network analysers at millimetre and sub-millimetre wavelengths", NPL Report TQE 5, National Physical Laboratory, Teddington, UK, March 2009.

[28] N. M. Ridler and R. G. Clarke, "Establishing Traceability to the International System of Units for Scattering Parameter Measurements from 750 GHz to 1.1 THz", IEEE Trans Terahertz Science & Technology, Vol 6, No 1, pp 2-11, January 2016.

[29] R. B. Marks, "A multi-line method of network analyzer calibration," IEEE Trans. Microwave Theory Tech., vol. 39, no. 7, pp. 1205–1215, July, 1991.

[30] D. F. Williams, C. M. Wang, and U. Arz, "An optimal vector-network-analyzer calibration algorithm", IEEE Trans. Microw. Theory Techn., vol. 51, no. 12, pp. 2391-2401, Dec. 2003. [28]

[31] N. M. Ridler and R. G. Clarke, "Investigating Connection Repeatability of Waveguide Devices at Frequencies from 750 GHz to 1.1 THz," Proc. 82nd ARFTG Microwave Measurement Conference, pp 87-99, Columbus, OH, USA, 20-21 November 2013

[32] N. M. Ridler and R. G. Clarke, "Further Investigations into Connection Repeatability of Waveguide Devices at Frequencies from 750 GHz to 1.1 THz", Proc. 83rd ARFTG Microwave Measurement Conference, pp 83-89, Tampa, FL, USA, 6 June 2014.

[33] N. M. Ridler and R. G. Clarke, "Evaluating the Effect of Using Precision Alignment Dowels on Connection Repeatability of Waveguide Devices at Frequencies from 750 GHz to 1.1 THz", *Proc. 84th ARFTG Microwave Measurement Conference*, pp 24-32, Boulder, CO, USA, 4-5 December 2014.

[34] T. Schrader; K. Kuhlmann; R. Dickhoff; J. Dittmer and M. Hiebel, "Verification of scattering parameter measurements in waveguides up to 325 GHz including highly-reflective devices", Adv. Radio Sci., Vol 9, pp 9-17, 2011.

[35] N. M. Ridler, M. J. Salter, "Cross-connected Waveguide Lines as Standards for Millimeter- and Submillimeter-wave Vector Network Analyzers," Proc. 81st ARFTG Microwave Measurement Conference, Seattle, WA, USA, 7 June 2013.

[36] Evaluation of measurement data - Guide to the expression of the Uncertainty in Measurement (GUM:1995), JCGM 100:2008, 1st ed., 2008, International Bureau of Weights and Measures (BIPM).

[37] N. M. Ridler, R. G. Clarke, R. D. Pollard, M. J. Salter, and A. Wilson, "Traceability to National Standards for S-parameter Measurements of Waveguide Devices from 110 GHz to 170 GHz," 73rd ARFTG Microwave Measurement Conference digest, pp 127-136, Boston Convention and Exhibition Center, Boston, MA, USA, 12 June 2009.

[38] N. M. Ridler, R. G. Clarke, M. J. Salter and A. Wilson, "Traceability to National Standards for S-parameter Measurements in Waveguide at Frequencies from 140 GHz to 220 GHz," 76th ARFTG Microwave Measurement Conference digest, pp 8-14, Marriott Suites on Sand Key, Clearwater Beach, FL, USA, 2-3 December 2010.

[39] N. M. Ridler, R. G. Clarke, M. J. Salter and A. Wilson, "Traceability to National Standards for S-parameter Measurements in Waveguide at Frequencies from 220 GHz to 330 GHz," 78th ARFTG Microwave Measurement Conference digest, pp 103-108, Tempe Mission Palms Hotel, Tempe, AZ, USA, 1 - 2 December 2011.

[40] M. Horibe and R. Kishikawa, "Metrological Traceability in Waveguide S-parameter Measurements at 1.0 THz Band," Instrumentation and Measurement, IEEE Transactions on, Volume 62, Issue: 6, pp 1814–1820, 2013.

[41] T. W. Crowe, B. Foley, S Durant, K. Hui, Y. Duan, J. L. Hesler, "VNA frequency extenders to 1.1 THz,", 36th International Conference on Infrared, Millimeter and Terahertz Waves (IRMMW-THz), 2011

[42] H.-W. Hübers, M. F. Kimmitt, N. Hiromoto, and E. Bründermann, "Terahertz Spectroscopy: System and Sensitivity Considerations", *IEEE Trans. THz Sci. Tech.,* 1 (2011) 321-331.

[43] M. Naftaly, ed., *Terahertz Metrology*, Artech House 2015.

[44] S. Mickan, J. Xu, J. Munch, X.-C. Zhang, and D. Abbott, "The limit of spectral resolution in THz time-domain spectroscopy," *Proc. SPIE*, vol. 5277, pp. 54–505, Mar. 2004.

[45] P. U. Jepsen and B. M. Fischer, "Dynamic range in terahertz time domain transmission and reflection spectroscopy," *Opt. Lett.*, vol. 30, pp. 29–31, 2005.

[46] M. Takeda, S. R. Tripathi, M. Aoki, and N. Hiromoto, "Exploration of the origin of random error in spectrum intensity measured with THz-TDS," in *Proc. 35th Int. Conf. Infrared Millim. Terahertz Waves*, 2010, pp. 1–2.

[47] N. Hiromoto, S. R. Tripathi, M. Takeda, and M. Aoki, "Study on random errors in THz signal and optical constants observed with THz time domain spectroscopy," in *Proc. 35th Int. Conf. Infrared Millim. Terahertz Waves*, 2010, pp. 1–2.

[48] D. A. Humphreys, M. Naftaly, "Dynamic range improvement of THz spectroscopy," *Precision Electromagnetic Measurements (CPEM 2014), 2014 Conference on*, pp.704-705, 24-29 Aug. 2014

[49] D. Jahn, S. Lippert, M. Bisi, L. Oberto, J. C. Balzer, M. Koch, "On the Influence of Delay Line Uncertainty in THz Time-Domain Spectroscopy", *J Infrared Milli Terahz Waves*, (2016).

[50] D. Grischkowsky, S. Keiding, M. van Exter, and C. Fattinger, "Far-infrared time-domain spectroscopy with terahertz beams of dielectrics and semiconductors," *Journal of the Optical Society of America B*, vol. 7, no. 10, pp. 2006–2015, 1990.

[51] L. Duvillaret, F. Garet, and J.-L. Coutaz, "A reliable method for extraction of material parameters in terahertz time-domain spectroscopy," *IEEE Journal of Selected Topics in Quantum Electronics*, vol. 2, no. 3, pp. 739–746, 1996.

[52] L. Duvillaret, F. Garet, and J.-L. Coutaz, "Highly precise determination of optical constants and sample thickness in terahertz time-domain spectroscopy," *Applied Optics*, vol. 38, no. 2, pp. 409–415, 1999.

[53] T. Dorney, R. Baraniuk, and D.Mittleman, "Material parameter estimation with terahertz time-domain spectroscopy," *Journal of the Optical Society of America A: Optics, Image Science, and Vision*, vol. 18, no. 7, pp. 1562–1571, 2001.

[54] I. Pupeza, R.Wilk, and M. Koch, "Highly accurate optical material parameter determination with THz time-domain spectroscopy," *Optics Express*, vol. 15, no. 7, pp. 4335–4350, 2007.

[55] M. Scheller, C. Jansen, and M. Koch, "Analyzing sub-100-μm samples with transmission terahertz time domain spectroscopy," *Optics Communications*, vol. 282, no. 7, pp. 1304–1306, 2009.

[56] W. Withayachumnankul, J. F. O'Hara, W. Cao, I. Al-Naib, and W. Zhang, "Limitation in thin-film sensing with transmission-mode terahertz time-domain spectroscopy", *Opt. Exp.* 22 (2014) 972-986.

[57] W. Withayachumnankul, B.M. Fischer and D. Abbott, "Material thickness optimization for transmission-mode terahertz time-domain spectroscopy", *Opt. Exp.* 16 (2008) 7382-7396.

[58] L. Duvillaret, F. Garet, and J.-L. Coutaz, "Influence of noise on the characterization of materials by terahertz time-domain spectroscopy", *J. Opt. Soc. Am. B,* 17 (2000) 452-461.

[59] M. Krüger. S. Funkner, E. Bründermann, M. Havenith, "Uncertainty and Ambiguity in Terahertz Parameter Extraction and Data Analysis", *J Infrared Milli Terahz Waves* 32 (2011) 699–715.

[60] O. Sushko, K. Shala, R. Dubrovka, and R. Donnan, "Revised metrology for enhanced accuracy in complex optical constant determination by THz-time-domain spectrometry", *J. Opt. Soc. Am. A,* 30 (2013) 979-986.

[61] P. Kužel, H. Němec, F. Kadlec, C. Kadlec, "Gouy shift correction for highly accurate refractive index retrieval in time-domain terahertz spectroscopy", *Opt. Exp.*, 18 (2010) 15338-15348.

[62] Q. Liang, G. Klatt, N. Krauß, O. Kukharenko, and T. Dekorsy, "Origin of potential errors in the quantitative determination of terahertz optical properties in time-domain terahertz spectroscopy," *Chin. Opt. Lett.* 13, (2015) 093001.

[63] W. Withayachumnankul, B.M. Fischer, H. Lin, D. Abbott, "Uncertainty in terahertz time-domain spectroscopy measurement", *J. Opt. Soc. Am. B,* 25 (2008) 1059-1072.

[64] Y. Shimada, H. Iida, M. Kinoshita, "Recent Research Trends of Terahertz Measurement Standards", *IEEE Trans. THz Sci. Tech.,* 5 (2015) 1166-1172.

[65] M. Naftaly, "Metrology issues and solutions in THz time-domain spectroscopy: Noise, errors, calibration," *IEEE Sensors J.*, 13 (2013) 8-17.

[66] M. Kinoshita, H. Iida, and Y. Shimada, "Frequency calibration of terahertz time-domain spectrometer using air-gap etalon," *IEEE Trans. THz Sci. Technol.*, 4 (2014) 756–759.

[67] Y. Deng, Q. Sun, J. Yu, "On-line calibration for linear time-base error correction of terahertz spectrometers with echo pulses", *Metrologia*, 51 (2014) 18-24.

[68] H. Iida, M. Kinoshita, Y. Shimada, H. Kuroda, K. Kitagishi, and Y. Izutani, "Validation of power linearity in terahertz time-domain spectroscopy using a programmable step attenuator," *IEEE Trans. Instrum. Meas.,* 62 (2013) 1801–1806.

[69] M. Naftaly, "An international intercomparison of THz time-domain spectrometers." Infrared, Millimeter, and Terahertz waves (IRMMW-THz), 2016 41st International Conference on. IEEE, 2016.

[70] B. Yang, X. Wang, Y. Zhang, R.S. Donnan, "Experimental characterization of hexaferrite ceramics from 100 GHz to 1 THz using vector network analysis and terahertz-time domain spectroscopy", *J Appl. Phys.*, 109 (2011) 033509.

[71] W. Sun, B. Yang, X. Wang, Y. Zhang, R.S. Donnan, "Accurate determination of terahertz optical constants by vector network analyzer of Fabry–Perot response", *Opt. Lett.*, 38 (2013) 5438-5441.

[72] T. Tosaka, K. Fujii, K. Fukunaga, A. Kasamatsu, "Development of complex relative permittivity measurement system based on free-space in 220-330 GHz range," *IEEE Trans. THz Sci. Tech.,* 5 (2015) 102-109.

[73] M. Naftaly, N. Shoaib, D. Stokes, N.M. Ridler, "Intercomparison of Terahertz Dielectric Measurements Using Vector Network Analyzer and Time-Domain Spectrometer", *J. Infrared Milli Terahz Waves*, 37 (2016) 691-702.

[74] M. R. Harper, A. J. A. Smith, M. A. Basu, D. A. Humphreys, "Calibration of a 70 GHz oscilloscope," *Proc. Conf. on Prec. Elect. Meas. (CPEM), London, UK*, pp. 530- 531, July 2004.

[75] A. J. A. Smith, A. G. Roddie, D. Henderson, "Electrooptic sampling of low temperature GaAs pulse generators for oscilloscope calibration," Opt. Quant. Elec., pp. 933-943, July 1996.

[76] M. Bieler, H. Fuser and K. Pierz, "Time-Domain Optoelectronic Vector Network Analysis on Coplanar Waveguides," IEEE Trans. Microwav. Theory and Tech., vol. MTT-63, no. 11, pp. 3775-3784, Nov. 2015.

[77] R. A. Dudley, A. G. Roddie, D. J. Bannister, A. D. Gifford, T. Krems and P Facon, "Electro-optic S-parameter and electric-field profiling measurement of microwave integrated circuits," IEE Proc. Sci Meas. Technol., vol. 146, no. 3, pp 117 – 122, May 1999.

[78] Y. Deng, H. Füser and M. Bieler, "Absolute Intensity Measurements of CW GHz and THz Radiation Using Electro-Optic Sampling," in IEEE Trans. on Instrumen. and Meas., vol. 64, no. 6, pp. 1734-1740, June 2015.

[79] P. D. Hale, D. F. Williams, A. Dienstfrey, J. Wang, J. Jargon, D. Humphreys, M. Harper, H. Füser, and M. Bieler, "Traceability of High-Speed Electrical Waveforms at NIST, NPL, and PTB," *Proc. Conf. on Prec. Elect. Meas. (CPEM),* Washington, USA, pp.522-523, July 2012.

[80] D.-J. Lee, J.-Y. Kwon, and N.-W. Kang, " Field analysis of electro-optic probes for minimally invasive microwave sampling," Opt. Express, vol. 22, no. 3, pp. 2897, Feb. 2014.

[81] S. Seitz, M. Bieler, G. Hein, K. Pierz, U. Siegner, F. J. Schmückle and W. Heinrich, "Characterization of an external electro-optic sampling probe: Influence of probe height on distortion of measured voltage pulses," J. of App. Phys.100, 113124, 2006.

[82] D. F. Williams, A.Lewandowski, T. S. Clement, J. C. M. Wang, P.D. Hale, J. M. Morgan, D. A. Keenan, and A. Dienstfrey, "Covariance-based uncertainty analysis of the NIST electrooptic sampling system," IEEE Trans. on Microwave Theory and Tech., vol. MTT-54, no. 1, pp. 481-491, Jan. 2006.

[83] H. Füser, S. Eichstädt, K. Baaske, C. Elster, K. Kuhlmann, R. Judaschke, K. Pierz and M. Bieler, "Optoelectronic time-domain characterization of a 100 GHz sampling oscilloscope," Meas. Sci. Technol. Vol. 23 025201, 2012.

[84] T. Hochrein, "Markets, availability, notice, and technical performance of terahertz systems: historic development, present, and trends." *Journal of Infrared, Millimeter, and Terahertz Waves* 36.3 (2015): 235-254.